NeuroImage 319 (2025) 121446

Contents lists available at ScienceDirect

NeuroImage

journal homepage: www.elsevier.com/locate/ynimg

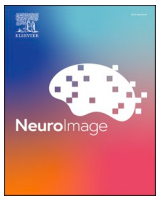

Rostro-caudal TMS mapping of immediate transcranial evoked potentials reveals a pericentral crescendo-decrescendo pattern

Marten Nuyts [a,b,1,*], Mikkel Malling Beck [a,1], Agata Banach [a], Axel Thielscher [a,c], Raf Meesen [b,d], Leo Tomasevic [a,e,f], Hartwig Roman Siebner [a,g,h,1], Lasse Christiansen [a,i,1,**]

[a] Danish Research Centre for Magnetic Resonance, Department of Radiology and Nuclear Medicine, Copenhagen University Hospital - Amager and Hvidovre, Copenhagen, Denmark, Kettegård Allé 30, 2650 Hvidovre, Denmark
[b] REVAL - Rehabilitation Research Center, Faculty of Rehabilitation Sciences, University of Hasselt, Diepenbeek, Belgium
[c] Department of Health Technology, Technical University of Denmark, Kgs. Lyngby, Denmark
[d] Movement Control and Neuroplasticity Research Group, Department of Movement Sciences, Group Biomedical Sciences, KU Leuven, Leuven, Belgium
[e] Department of Psychiatry and Psychotherapy, University of Regensburg, Regensburg, Germany
[f] Department of Human Sciences, Institute of Psychology, University of the Bundeswehr Munich, Neubiberg, Germany
[g] Department of Neurology, Copenhagen University Hospital - Bispebjerg and Frederiksberg, Bispebjerg Bakke 23, 2400 København NV, Denmark
[h] Department of Clinical Medicine, Faculty of Health and Medical Sciences, University of Copenhagen, Blegdamsvej 3B, 2200 Copenhagen N, Denmark
[i] Institute of Neuroscience, University of Copenhagen, Blegdamsvej 3B, 2200 Copenhagen N, Denmark

ARTICLE INFO

Keywords:
Transcranial magnetic stimulation (TMS)
Electroencephalography (EEG)
TMS-EEG
Immediate transcranial evoked potential (iTEP)

ABSTRACT

Background: We recently demonstrated that single-pulse TMS of the primary sensorimotor hand area ($SM1_{HAND}$) elicits an immediate transcranial evoked potential (iTEP). This iTEP response appears within 2–8 ms post-TMS, featuring high-frequency peaks superimposed on a slow positive wave. Here, we used a linear TMS-EEG mapping approach to characterize the rostro-caudal iTEP expression and compared it to that of motor-evoked potentials (MEPs).

Methods: In 15 healthy young volunteers (9 females), we identified the iTEP hotspot in left $SM1_{HAND}$. We applied single biphasic TMS pulses at an intensity of 110 % of resting motor threshold over six cortical sites along a rostro-caudal axis (2 cm rostral to 3 cm caudal to the $SM1_{HAND}$ hotspot). We analyzed site-specific iTEP and MEP responses.

Results: iTEP magnitude decreased rostrally and caudally from the $SM1_{HAND}$ hotspot. MEPs exhibited a similar rostro-caudal crescendo-decrescendo pattern. While iTEP and MEP response profiles were similar, normalized iTEP amplitudes decayed less rapidly at the first postcentral site.

Discussion: These findings support the idea that pericentral iTEPs reflect a direct response signature of the pericentral cortex, possibly involving a synchronized TMS-induced excitation of cortical pyramidal tract neurons. Similar but non-identical rostro-caudal patterns suggest that iTEPs and MEPs may arise from overlapping but distinct neuronal populations.

1. Introduction

Transcranial magnetic stimulation (TMS) synchronously excites cortical neurons, and neuronal excitation propagates transsynaptically through cortico-cortical and cortico-subcortical pathways (Siebner et al., 2022). Simultaneous electroencephalography (EEG) captures these transcranially evoked potentials (TEPs), reflecting the temporospatial dynamics of TMS induced activation of local and remote brain

* Corresponding author at: Hasselt University, Faculty of Rehabilitation Sciences, Universiteit Hasselt, Campus Diepenbeek, Faculteit Revalidatiewetenschappen, Wetenschapspark 7, B-3590 Diepenbeek.
** Corresponding author at: Danish Research Centre for Magnetic Resonance, Centre for Functional and Diagnostic Imaging and Research, Copenhagen University Hospital - Amager and Hvidovre, Kettegård Allé 30, 2650 Hvidovre, Denmark.
E-mail addresses: marten.nuyts@uhasselt.be (M. Nuyts), lassec@drcmr.dk (L. Christiansen).
[1] Shared authorship

https://doi.org/10.1016/j.neuroimage.2025.121446
Received 21 March 2025; Received in revised form 2 September 2025; Accepted 5 September 2025
Available online 6 September 2025

regions (Ilmoniemi et al., 1997; Hernandez-Pavon et al., 2023), offering insights into cortical excitability and connectivity (Beck et al., 2024; Farzan and Bortoletto, 2022). Measuring the immediate cortical response to single-pulse TMS has been challenging, as the EEG signal within the first 10 milliseconds was obscured by various artifacts generated by the TMS pulse (Veniero et al., 2009; Tomasevic et al., 2017) and scalp muscle activity (Mutanen et al., 2013).

Using single-pulse TMS over the left primary sensorimotor hand area ($SM1_{HAND}$), we recently demonstrated the feasibility of recording immediate transcranial evoked potentials (iTEPs) as early as 2–3 ms post-stimulation (Beck et al., 2024). A subsequent study confirmed the presence of iTEPs using a different TMS-EEG setup (Stango et al., 2024). These responses feature high-frequency peaks (650–900 Hz inter-peak frequency) superimposed on a slower wave. The short latencies of iTEPs align with evoked neuronal activity recorded invasively in non-human primates (Mueller et al., 2014), possibly reflecting the excitation of large pyramidal neurons. The rhythmicity of the high-frequency iTEP components resembles TMS-evoked descending corticospinal volleys, that can be recorded with epidural electrodes (Di Lazzaro and Rothwell, 2014). Notably, iTEP inter-peak intervals mirror those observed when probing short-interval intracortical facilitation (SICF) with paired-pulse TMS of $SM1_{HAND}$ and measuring motor-evoked potentials (MEPs) in the contralateral hand muscles (Ziemann et al., 1998). Establishing iTEPs as a direct marker of cortical excitability enhances the utility of the TMS-EEG approach, as later TEP components likely reflect secondary activation in local and remote brain regions, alongside non-transcranial co-activations via multisensory peripheral inputs (Bortoletto et al., 2015; Conde et al., 2019).

In our initial report, iTEPs were found to depend on TMS intensity and current direction (Beck et al., 2024). Moreover, iTEPs could only be elicited from the $SM1_{HAND}$ region and not from posterior parietal or midline areas, despite identical stimulation parameters. While these findings might suggest that iTEPs are a characteristic response feature of the sensorimotor cortex, this remains to be systematically investigated.

This study aimed to map the spatial expression of pericentrally evoked iTEPs along a rostro-caudal gradient. Using the same target region as in previous iTEP studies (Beck et al., 2024; Stango et al., 2024), we stimulated six frontoparietal cortical sites, spaced 1 cm apart, spanning 2 cm rostral to 3 cm caudal from the left $SM1_{HAND}$. Since the neural circuitries generating high-frequency cortical activity (650–900 Hz) are thought to reside in the pericentral cortex (Ziemann, 2020), we hypothesized that iTEPs would peak over $SM1_{HAND}$ and gradually decline with increasing distance in both, the rostral and caudal direction. Concurrently, we recorded MEPs from two contralateral intrinsic hand muscles to examine the spatial alignment and separation of iTEP- and MEP-generating sites with our linear TMS mapping approach. Lastly, we explored the rostro-caudal expression of later TEP components and their relationship with iTEPs.

2. Methods

2.1. Participants

A total of 17 healthy volunteers (10 females; mean age: 27; range: 20–35) were initially recruited to participate. Participants were excluded in case of (1) contraindications for TMS or MRI; (2) a known neurological disease or psychiatric disorder; (3) coactivation of scalp muscles following a tailored $SM1_{HAND}$ hotspot procedure (see below). Since higher absolute TMS intensities are more prone to coactivate scalp muscles, participants were partly, but not exclusively, recruited based on their resting motor threshold (rMT). It was possible to collect scalp muscle artifact-free data in 15 out of the 17 individuals tested. All participants provided written informed consent prior to participation, following the Declaration of Helsinki. The protocol was approved by the regional ethical committee (Capital Region of Denmark; Protocol number H-15008824).

2.2. Experimental design

A tailored $SM1_{HAND}$ hotspot procedure was used (for details, see (Beck et al., 2024) and Fig. 1) to allow the recording of the earliest EEG responses following TMS. The left motor hand knob area, identified on the individual's T1-weighted image, was used as a starting point for stimulation (Yousry et al., 1997). Starting from the motor hand knob area, the coil was moved in small steps to locate the stimulation site with the largest and most consistent MEP amplitudes in the FDI muscle, designated as the 'MEP hotspot' (Fig. 1). Over the MEP hotspot, we determined the individual resting motor threshold (rMT), defined as the lowest stimulation intensity capable of eliciting peak-to-peak MEP amplitudes of $\geq$50 μV in at least 5 out of 10 consecutive trials. Next, while stimulating at 110 % rMT, 10–20 averaged EEG trials were visually inspected in real time using BrainVision Recorder Software to assess for scalp muscle artifacts (Casarotto et al., 2022). Scalp muscle artifacts were identified based on their characteristic topography, morphology, and amplitude. When targeting $SM1_{HAND}$, scalp muscle artifacts typically appear over fronto-temporal electrodes, show a distinctive bipolar waveform resembling compound muscle action potentials, and often exceed the amplitudes of TEPs (Beck et al., 2024). If no scalp muscle artifacts were observed, which was the case for 10 out of 17 subjects, the MEP hotspot was set as the $SM1_{HAND}$ stimulus location. When scalp muscle artifacts were identified, small adjustments in the coil's position and tilt were made towards the midline in search for an alternate stimulus location, where MEPs could be evoked without concurrent scalp muscle activation (Mutanen et al., 2013). This position was designated as the "TEP-optimized $SM1_{HAND}$ hotspot". Over the TEP-optimized $SM1_{HAND}$ hotspot, we reassessed the individual rMT and the absence of scalp muscle artifacts using that location's target intensity of 110 %rMT. If no scalp muscle artifacts were observed, the TEP-optimized $SM1_{HAND}$ hotspot was defined as the $SM1_{HAND}$ stimulus location. This was the case for 5 out of 7 remaining subjects. For the remaining 2 participants, we were unable to identify a scalp muscle artifact-free stimulation location.

In 15 participants (9 females; mean age: 27; range: 20–35), data were collected over six frontoparietal cortical sites along a rostro-caudal line using a stimulation intensity of 110 %rMT (Fig. 1). Each stimulus location was spaced 1 cm apart, moving up to a maximum of 2 cm rostral to 3 cm caudal from $SM1_{HAND}$. Stimulation was applied in a sequential order, starting with $SM1_{HAND}$ and proceeding to rostro-caudal stimulation sites 1 cm, 2 cm, and 3 cm from $SM1_{HAND}$, respectively. We initially set out to also include a stimulation site 3 cm rostral from $SM1_{HAND}$, but according to pilot-testing, this was not feasible due to scalp muscle coactivation by TMS. In line with the procedure outlined for the $SM1_{HAND}$ stimulation site above, each rostro-caudal stimulus location was first visually checked for scalp muscle coactivation (Fig. 1). If scalp muscle artifacts were observed, small medial coil adjustments were made. This was only the case for two subjects when moving 1 cm (SUB-09) and/or 2 cm (SUB-02 and SUB-09) rostral from $SM1_{HAND}$. For one participant (SUB-12), the rMT was 97 % of the maximum stimulator output (MSO), precluding stimulation at 110 % rMT. As a result, stimulation had to be delivered at 100 % of MSO, the highest available suprathreshold intensity. This participant was excluded from the correlations presented in Sections 2.6.3 and 3.3., as lower relative intensities yielded smaller iTEPs (Beck et al., 2024) and TEPs (Beck et al., 2023; Kähkönen et al., 2005), potentially inflating potential associations.

2.3. Transcranial magnetic stimulation (TMS)

Over each stimulus location, single TMS pulses were delivered every 2 s (± 10 % jitter) using a 35 mm figure-of-eight coil (MC-B35 coil, MagVenture X100 with MagOption, MagVenture A/S, Farum, Denmark) coated with a layer of foam (± 1.5 mm thick). The coil was placed tangentially to the scalp and oriented approximately 45° to the midline,

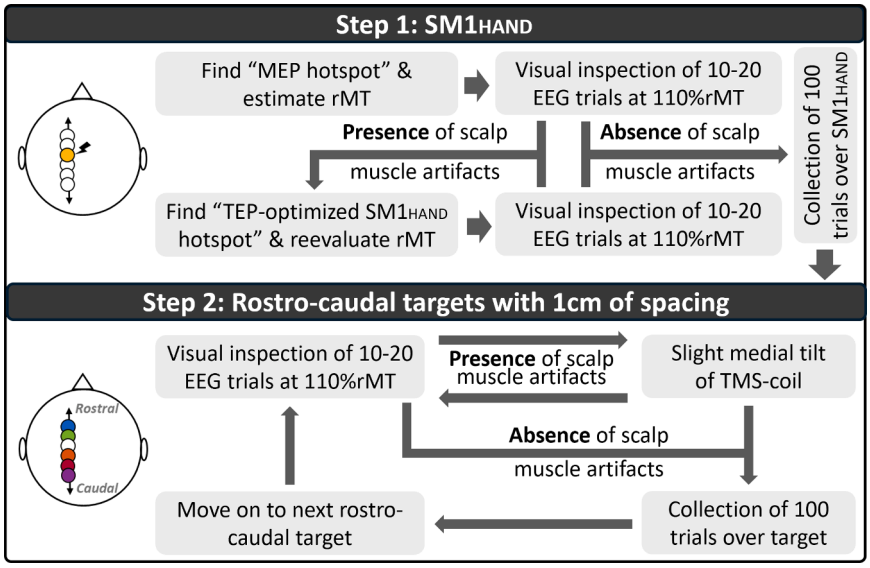

Fig. 1. Procedure for collecting a scalp muscle artifact-free dataset at each stimulation site. Step 1 involved identifying the optimal stimulation site where the largest motor-evoked potential (MEP) could be elicited without coactivation of scalp muscles. Small adjustments in coil position and tilt were made if needed. Step 2 involved collecting data along a rostro-caudal line centered around the (TEP-optimized) primary sensorimotor hand area ($SM1_{HAND}$) stimulus location identified in step 1. The coil was tilted slightly medially if scalp muscle coactivation occurred.

with the coil handle pointing backwards. A biphasic pulse configuration, inducing an antero-posterior to postero-anterior (AP-PA) current in the brain, was used to lower the absolute TMS intensity required (Kammer et al., 2001; Sommer et al., 2006). The recharge delay of the stimulator was set to 500 ms post-TMS. Stereotaxic neuronavigation (TMS Navigator, Localite, GmbH, Bonn, Germany) tracked the position, tilt, and orientation of the TMS coil throughout the experiment. In eight participants, structural brain scans were acquired with a 3T PRISMA scanner (Siemens, Erlangen, Germany), while in nine participants a 3T Achieva scanner (Philips, Best, The Netherlands) was used.

2.4. Electroencephalography (EEG) and electromyographic (EMG) recordings

EEG was recorded from the scalp with 61 passive Ag/AgCl TMS-compatible electrodes embedded in an equidistant EEG cap (M10 cap layout, BrainCap TMS, Brain Products GmbH, Germany) with the ground and reference electrodes placed on the left and right side of the individual's forehead, respectively. To keep impedance levels below 5 kΩ, electrodes were prepared with an electroconductive abrasive gel and routinely checked throughout the experiment. Data were recorded with BrainVision Recorder software (Brain Products GmbH, Germany) and a TMS-compatible EEG amplifier (actiCHamp Plus 64 System, Brain Products GmbH, Germany) set at a sampling frequency of 50 kHz (anti-aliasing low-pass filter at 10.300 Hz). A very high sampling frequency was chosen to shorten the duration of the TMS pulse artifact to ± 2 ms (Beck et al., 2024). Participants were asked to keep their eyes open, minimize blinking, and relax their face throughout the experiment.

Electromyographic (EMG) activity was simultaneously recorded from the first dorsal interosseus (FDI) and adductor digiti minimi (ADM) muscles of the right hand via self-adhesive surface electrodes (Ambu Neuroline 700) placed on the prepared skin. A belly-tendon montage was used with the ground positioned over the right styloid process of the ulna. EMG signals were amplified (gain = 1000) (Digitimer D360, Digitimer Ltd., Hertfordshire, UK), 0.02 – 2 kHz bandpass filtered, digitized at 5 kHz (CED 1401 micro, CED Limited, Cambridge, UK), acquired via Signal software (Cambridge Electronic Design), and stored for offline analyses.

During blocks of data-collection, pink noise, intermixed with pre-recorded TMS-clicks, was played through modified earplugs to minimize the effect of the TMS-clicking sounds. Sound mask was generated using the TMS Adaptable Auditory Control (TAAC) software (Russo et al., 2022).

2.5. Data analysis

All data were preprocessed and analyzed offline using custom MATLAB scripts (2022b, The Math-Works Inc., Portola Valley, California, USA) using EEGLAB (Delorme and Makeig, 2004) and Fieldtrip functions (Oostenveld et al., 2011).

EMG data were visually checked for background muscle activity in a window of 100 ms pre-stimulus. Single trials containing background EMG activity were discarded prior to averaging from the EMG and EEG dataset (median: 1; range: 0–28), as were bad channels in the EEG dataset (see **Table S1** for an overview). Peak-to-peak MEP amplitudes from the right FDI muscle were calculated over each stimulus location as the difference between the maximum and minimum values from 20 ms to 40 ms post-stimulus from the average trace.

EEG data were epoched from −500 ms to 500 ms around the stimulus, baseline corrected from a window of −110 ms to −10 ms from the stimulus, band-pass filtered (2nd order zero-phase Butterworth filter at 0.1–2000 Hz), and averaged. Following these steps, the global mean field power (GMFP) was computed (Lehmann and Skrandies, 1980), as it serves as a general activation index, aimed at avoiding potential spatial bias from single-channel(s) extraction related to the stimulus location. The GMFP was computed with decay artifact channels included and removed. To characterize the high-frequency component of iTEPs, we calculated the difference between the first two peaks relative to the first trough and the third peak relative to the second trough (**Table S2**). Peaks and troughs were calculated over each stimulation location as the local minimum and maxima values from 2 ms to 8 ms post-stimulus from the average trace, with a minimal peak or trough interval of 1 ms.

2.6. Statistical analysis

Statistical analysis of all data was performed in MATLAB and R, using RStudio (lme4 package) (RStudio, 2021; RStudio, 2020; Patil, 2021; Bates et al., 2015). For simplification, intercepts and error terms are not explicitly reported here but were included in all models. Alpha was set at 0.05, and all P-values were two-tailed. When relevant, Tukey- or

Bonferroni-corrected post-hoc comparisons were performed.

2.6.1. The effect of stimulus location on iTEPs

The effect of stimulus location on iTEPs was examined by applying a temporal clustering approach, with a mixed effect model fitted for each timepoint within a window of 2–8 ms post-stimulation (Van Hoornweder, 2025). The mixed models included STIMULATION SITE (six levels, six frontoparietal locations) as a fixed factor, PARTICIPANT as the random intercept, and GMFP as the dependent variable:

$$GMFP_{ij} = \beta_1 STIMULATION\ SITE_{ij} \tag{1}$$

F-values were extracted for each model and used to calculate threshold-free clustering enhanced (TFCE) values (Smith and Nichols, 2009):

$$TFCE = \int_h e(h)^E h^H dh \tag{2}$$

Where h represents cluster height (F-value threshold), e denotes cluster extent (number of temporally adjacent data points $> h$), and H and E are their respective weights, with default values of $H = 2$ and $E = 0.5$. h was incrementally increased from 0 in steps of 0.2 until the maximum F-value was reached. Significance was derived if TFCE values surpassed the 95th percentile of a surrogate null distribution generated from 800 permutations (Van Hoornweder, 2025). By using TFCE, we identified significant differences in iTEPs across stimulus locations over time without performing independent tests at predefined time points.

2.6.2. The relationship between iTEPs and MEPs

The relationship between MEPs and iTEPs was assessed using three complementary analyses. All analyses included normalization procedures to account for individual and measurement variability and aid comparisons between excitability measures.

In the first analysis, we normalized rostro-caudal excitability profiles to each individual's peak response. Specifically, for each individual excitability measure (MEP, iTEP peak 1 – trough 1, and iTEP peak 2 – trough 1), the amplitude at each location was normalized by dividing it by the amplitude at the stimulation site with the highest response for that individual. Next, a mixed model was derived with AMPLITUDE as the dependent variable and PARTICIPANT included as the random intercept. STIMULATION SITE (six levels, six frontoparietal sites) and EXCITABILITY MEASURE (three levels: MEP; iTEP peak 1 – trough 1; iTEP peak 2 – trough 1) were added as main effects and in interaction with each other:

$$\begin{aligned} AMPLITUDE_{ijk} = {} & \beta_1 STIMULATION\ SITE_{ij} \\ & + \beta_2 EXCITABILITY\ MEASURE_{ik} \\ & + \beta_3 (STIMULATION\ SITE_{ij} \\ & \times EXCITABILITY\ MEASURE_{ik}) \end{aligned} \tag{3}$$

We did not include iTEP peak 3 - trough 2 as a level to EXCITABILITY MEASURE, as this metric could only be extracted in 4 out of 15 participants (see results below).

In the second analysis, we computed an amplitude-weighted mean position for each excitability measure along the rostro-caudal line for each subject (Raffin et al., 2015), designated as the weighted mean position (WMP):

$$WMP = \frac{\sum_{k=1}^{6} Stimulus\ site\ (k)\ *\ Mean\ amplitude\ (k)}{\sum_{k=1}^{6} Mean\ amplitude\ (k)} \tag{4}$$

Where "Stimulation site (k)" refers to each of the six stimulation sites, while "Mean amplitude (k)" is calculated from the peak-to-peak amplitudes of MEPs or peak-to-trough amplitudes of iTEPs at each of the six stimulation sites. In doing so, the WMP was calculated for three excitability measures: MEP, iTEP peak 1 – trough 1, and iTEP peak 2 – trough 1. To investigate differences in WMP between MEPs and iTEPs, a mixed model was derived with WMP as dependent variable, PARTICIPANT as the random intercept and EXCITABILITY MEASURE (three levels: MEP; iTEP peak 1 – trough 1; iTEP peak 2 – trough 1) added as a fixed factor:

$$WMP_{ij} = \beta_1 EXCITABILITY\ MEASURE_{ij} \tag{5}$$

Lastly, the association between the WMP of MEPs and iTEP peaks was tested using a multiple linear regression model:

$$MEP_i = \beta_1 PEAK1_i + \beta_2 PEAK2_i \tag{6}$$

2.6.3. The effect of stimulus location on TEPs and their relationship to iTEPs

To assess the site-specificity of TEPs, we first applied a temporal clustering approach across a post-stimulation window of 2–200 ms, using the same mixed model employed for the iTEPs (see Eq. (1)). To assess the site-specificity of TEPs, we first applied a temporal clustering approach across a post-stimulation window of 2–200 ms, using the same mixed model employed for the iTEPs (see Eq. (1)). Because temporal clustering may overlook variability in later TEP components, we conducted complementary analyses. We extracted absolute peak amplitudes within time windows corresponding to canonical TEP components (i.e., N15, P30, N45, P60, and N100) (Beck et al., 2024). For each component, we fitted a separate mixed-effects model with TEP amplitude as the dependent variable, STIMULATION SITE (six frontoparietal sites) as the fixed effect, and PARTICIPANT as a random intercept:

$$TEP_{ij} = \beta_1 STIMULATION\ SITE_{ij} \tag{7}$$

Both the temporal clustering and mixed model analyses revealed a site-specific effect only for the N15 component. Subsequent analyses were therefore restricted to the N15, quantified as the area under the curve (AUC) within the significant time window. Specifically, its spatial relationship with iTEPs was assessed by mirroring the approach previously applied to iTEPs and MEPs (see Section 2.6.2.). First, we normalized the N15 rostro-caudal excitability profile to each individual's highest response (see Section 2.6.2.). Accordingly, we compared the normalized rostro-caudal excitability profiles between the iTEPs peaks and the N15 (see Eq. (3)). Second, we investigated the differences in WMP between iTEPs and N15 (see Eq. (4)). Third, the association between the WMP of N15 and the iTEP peaks was tested using a multiple linear regression model:

$$N15_i = \beta_1 iTEP\ PEAK1_i + \beta_2 iTEP\ PEAK2_i \tag{8}$$

Lastly, an exploratory analysis assessed the relationship between later TEP peaks and iTEP peak-to-trough amplitude. The analysis was limited to TEPs evoked from $SM1_{HAND}$, since changes in the rostro-caudal coil position inevitably introduced the same changes in all TEPs that share a spatial excitability center of gravity. For each TEP peak, we fitted a general linear model with TEP amplitude as the dependent variable. iTEP peak 1 – trough 1 and iTEP peak 2 – trough 1 were added as main effects, as well as in interaction with each other:

$$\begin{aligned} TEP_{ijk} = {} & \beta_1 iTEP\ PEAK1_{ij} + \beta_2 iTEP\ PEAK2_{ik} \\ & + \beta_3 (iTEP\ PEAK1_{ij} \times iTEP\ PEAK2_{ik}) \end{aligned} \tag{9}$$

3. Results

Single-pulse stimulation over six frontoparietal cortical sites (Fig. 2**A**) resulted in MEPs in both hand muscles by stimulating in the proximity of the hand region. The iTEPs were evoked in all 15 subjects (**Figure S1**), characterized by a series of 2–3 peaks with an underlying slower component. Fig. 2 illustrates the averaged response for iTEPs (Fig. 2**B** and 2**C**), their averaged topographical distribution between the first and second iTEP peak (Fig. 2**D**), the averaged MEPs in both hand muscles (Fig. 2**E**), and the averaged response for later TEP components (Fig. 2**F**). In addition to Fig. 2, we recomputed the averaged iTEP

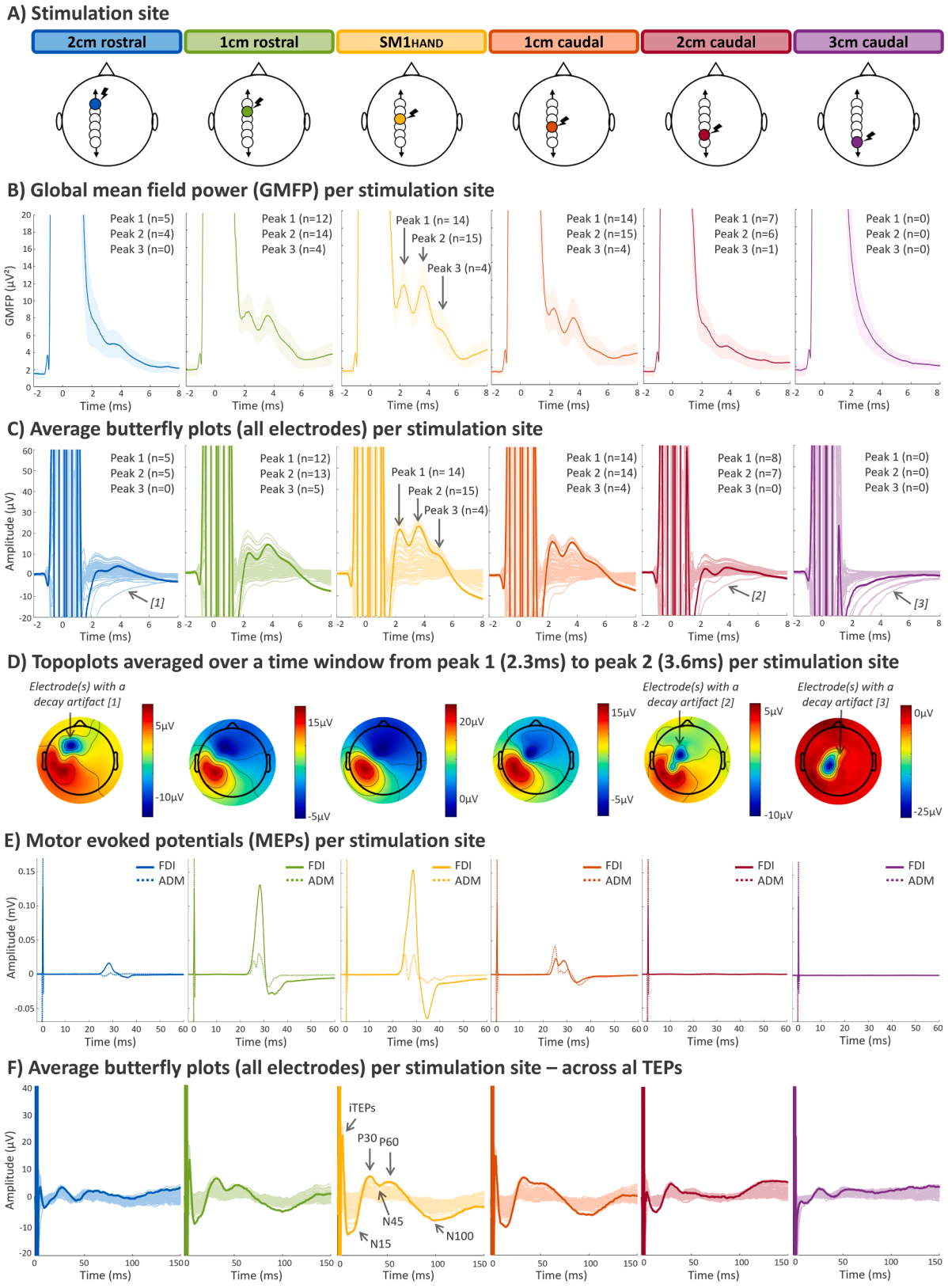

Fig. 2. Immediate transcranial evoked potentials (iTEPs) and motor-evoked potentials (MEPs) across stimulation sites. **(A)** The six rostro-caudal sites of stimulation centered around the sensorimotor hand area ($SM1_{HAND}$). **(B)** Global mean field power (GMFP), showing that iTEPs are maximally expressed following stimulation over pericentral stimulation sites. **(C)** Average butterfly plots with the electrode closest to $SM1_{HAND}$ highlighted, showing that iTEPs are maximally expressed at pericentral stimulation sites. Decay artifact channels are indicated by arrows. **(D)** Topoplots, averaged over a time window from iTEP peak 1 to peak 2 (i.e., 2.3 ms – 3.6 ms). Decay artifact channels are indicated by arrows. **(E)** MEPs of the right first dorsal interosseus (FDI) and abductor digiti minimi (ADM) indicated by solid and dashed lines, respectively. MEP peak-to-peak amplitudes were greatest following stimulation over central sites. **(F)** Average butterfly plots across all TEPs with the electrode closest to $SM1_{HAND}$ highlighted.

response with decay artifact channels removed as shown in the supplementary materials (**Figure S2**).

3.1. The effect of stimulus location on iTEPs

Decay artifacts were present in some EEG channels after stimulation (Fig. 2**C**), and this contaminated the group average EEG data and the topographical distribution of the EEG response (Fig. 2**D**). Using a stepwise procedure, we identified and removed channels exhibiting a decay artifact for longer than 2 ms post-stimulation (see **Figure S3** for details). Accordingly, the effect of stimulus location on iTEPs was tested using two separate temporal clustering analyses, with and without decay artifact channels included. Both analyses provided statistical support for previous observations of changes in iTEPs across stimulus locations.

A first temporal clustering analysis, with decay artifacts channels included, revealed a significant difference between stimulation sites driven by a cluster from 3.22 ms to 4.42 ms post-TMS (Fig. 3**A**). The median GMFP amplitude was highest when stimulating over $SM1_{HAND}$ (10.16 μV^2), followed by 1 cm rostral (7.54 μV^2), 1 cm caudal (6.90 μV^2), 2 cm rostral (4.88 μV^2), 3 cm caudal (4.34 μV^2), and finally 2 cm caudal (4.22 μV^2) from $SM1_{HAND}$. The same temporal clustering analysis, but with decay artifact channels removed, revealed a significant difference between stimulation sites driven by a cluster from 2.18 ms to 4.42 ms post-TMS (Fig. 3**B**). The median GMFP amplitude was when the coil was placed over $SM1_{HAND}$ (9.67 μV^2), followed by 1 cm rostral (7.31 μV^2), 1 cm caudal (6.76 μV^2), 2 cm rostral (4.20 μV^2), 2 cm caudal (3.71 μV^2), and finally 3 cm caudal (2.33 μV^2) from $SM1_{HAND}$.

3.2. The relationship between iTEPs and MEPs

Since decay artifacts can (1) obscure the detection of iTEP peaks (**Figure S4**) and (2) alter the time window for detecting effects (Fig. 3), all analyses examining the relationship between iTEPs and MEPs were conducted using the decay-artifact free data. Overall, we statistically confirm a spatial relationship between MEPs and iTEP peaks, while identifying several important differences.

First, iTEPs and MEPs were elicited concurrently over most (central) stimulus locations, although iTEPs could be elicited in the absence of MEPs during rest (Fig. 4**A**). Second, Fig. 4**B** illustrates the normalized excitability profiles for both iTEPs and MEPs. A mixed model investigating the effect of stimulation site on these rostro-caudal excitability profiles revealed a significant two-way interaction between STIMULATION SITE and EXCITABILITY MEASURE ($F_{10,238} = 2.39$, $p = 0.01$). Specifically, post-hoc testing revealed significant differences between the normalized MEP amplitude and both iTEP peak 1 – trough 1 ($t = -4.91$, $p < 0.001$) and iTEP peak 2 – trough 1 ($t = -4.37$, $p = 0.002$) when the coil was positioned 1 cm caudal from $SM1_{HAND}$, as can be observed in Fig. 4**B** In accordance with this result, we observed a median caudal difference of 1.4 mm in the WMP from the first iTEP peak relative to the MEP (Fig. 4**C**), though the effect of EXCITABILITY MEASURE on WMP did not reach statistical significance ($F_{2,28} = 3.02$, $p = 0.065$). Nevertheless, a numerical indication was prevalent, with 12 out of 15 subjects showing a more caudal WMP of the first iTEP peak relative to the MEP. Additionally, an overall moderate linear relationship was observed between the WMP of MEPs and iTEP peaks (Fig. 4**D**), with an R^2 of 0.54. Collectively, these results suggest that iTEPs expression resembled that of the MEP, albeit slightly caudal.

Exploratory analyses revealed a systematic median increase in the onset latency of the MEP and the peak latency of the late iTEP peaks as the coil was centered away from $SM1_{HAND}$ (**Figure S4** and **Table S3**). The analyses and results are described and discussed in the supplementary materials.

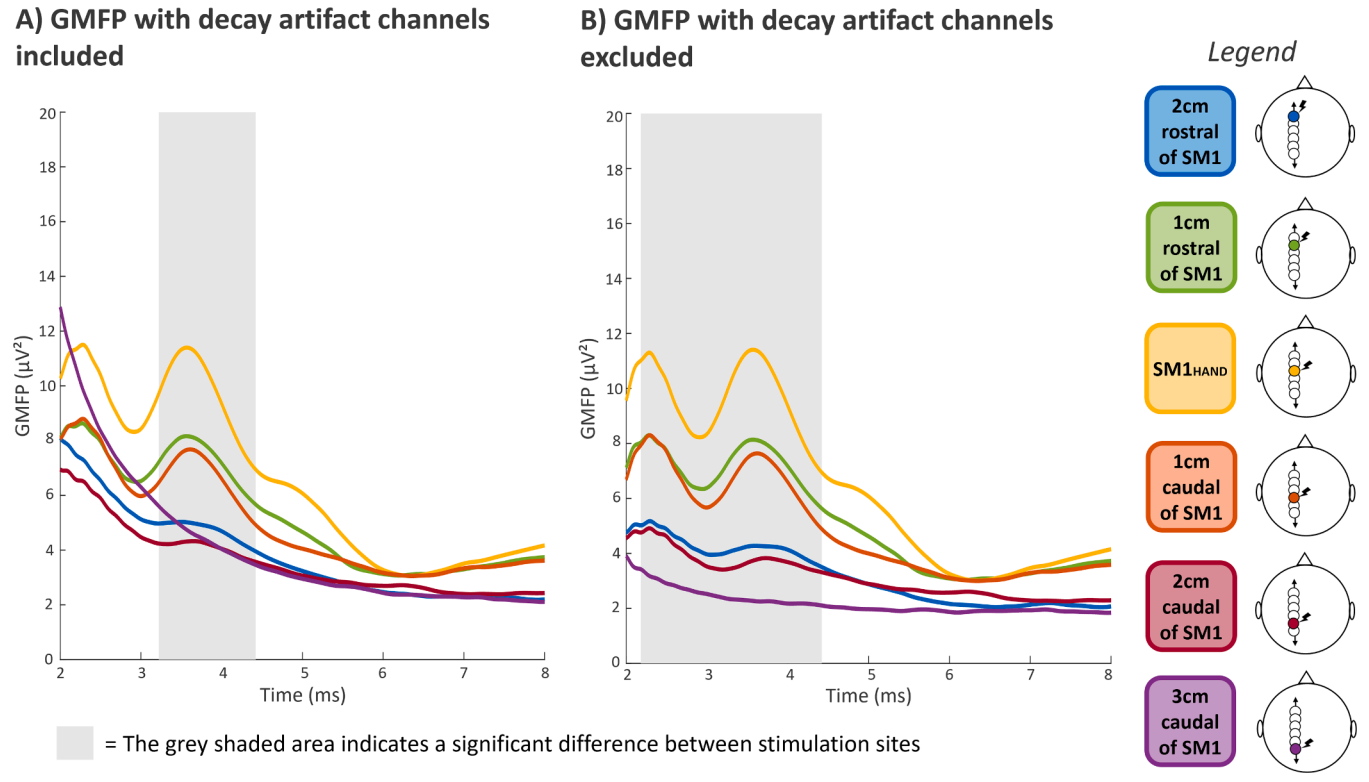

Fig. 3. The effect of stimulation site on immediate transcranial evoked potentials (iTEPs), analyzed from 2 ms to 8 ms post-stimulation. The grey shaded area indicates a significant difference in global mean field power (GMFP) between stimulation sites. **(A)** GMFP with decay artifact channels included. **(B)** GMFP with decay artifact channels excluded.

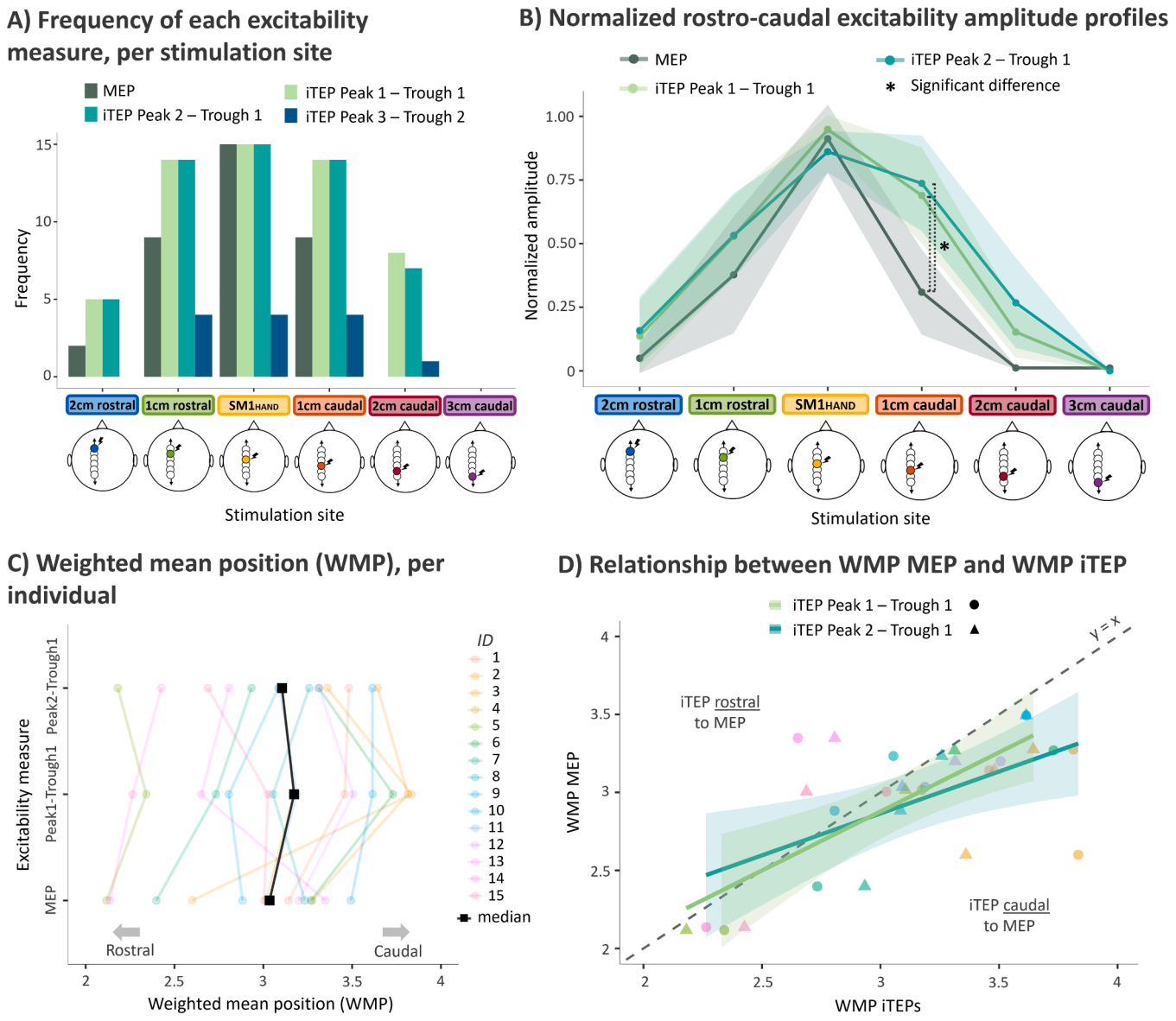

Fig. 4. Relationship between the amplitude of immediate transcranial evoked potentials (iTEPs) and motor-evoked potentials (MEPs). **(A)** Histograms showing the presence of MEPs and iTEP responses at each stimulation site across subjects. **(B)** Normalized rostro-caudal excitability amplitude profiles, illustrating the significant EXCITABILITY MEASURE by STIMULATION SITE interaction. **(C)** Weighted mean position (WMP) for each excitability measure shown per subject, with black squares indicating the median WMP for each measure. **(D)** Association between the WMP of MEPs and each iTEP peak, showing a strong, but slight caudal, relationship.

3.3. The effect of stimulus location on standard TEP components at later latencies and their relationship with iTEPs

In addition to the iTEPs, single-pulse stimulation over six fronto-parietal cortical sites reliably evoked a series of well-known early and later TEP components (Fig. 2**F**). These later TEP components were evoked in all subjects, albeit varying in size and latency (**Figure S5**). While some subjects showed both clear iTEP and prototypical TEP peaks, other participants showed clear iTEP peaks over multiple stimulus locations but did not express most of the later TEP peaks. **Figure S6** illustrates the averaged TEP waveforms and corresponding topographical distributions across all stimulation sites.

A temporal clustering analysis on all TEPs revealed a significant difference of the early TEP component among stimulation sites, consistent with the findings from the iTEP analysis (see Section 3.1 and Fig. 3). Additionally, a significant early cluster was identified between 7.72 ms and 18.44 ms post-TMS (**Figure S7A**), matching the time-window for the prototypical early N15 peak (**Figure S8**). In this cluster, the median GMFP amplitude was highest when stimulating over $SM1_{HAND}$ (4.52 μV^2), followed by 1 cm caudal (4.39 μV^2), 1 cm rostral (4.05 μV^2), 2 cm caudal (2.46 μV^2), 2 cm rostral (2.24 μV^2), and 3 cm caudal (1.87 μV^2) from $SM1_{HAND}$. Consistent with this result, mixed models revealed a site-specific effect only for the N15 peak ($F_{5,70} = 4.82$, $p < 0.005$), with no significant effects for later components (all $p > 0.23$) after Bonferroni correcting for multiple comparisons.

To explore the site-specific effect of the N15 in more detail, we compared its normalized magnitude profile to that of iTEPs. **Figure S7B** illustrates an overall spatial overlap between iTEP and N15 normalized excitability profiles. Accordingly, a mixed model investigating the effect of stimulation site on the iTEP and N15 normalized rostro-caudal excitability profiles revealed a significant two-way interaction between STIMULATION SITE and EXCITABILITY MEASURE ($F_{10,252} = 3.68$, $p < 0.001$). Although post-hoc testing revealed a significant difference between the N15 with the first ($t = 4.36$, $p = 0.003$) and second

($t = 4.36$, $p = 0.003$) iTEP peak when the coil was positioned 3 cm from $SM1_{HAND}$, this is most likely due to residual noise at the N15 time window and is supported by the lack of an N15 peak at this stimulation site (**Figure S7A**). We next compared the WMP of the N15 and iTEP peaks, revealing a significant main effect of EXCITABILITY MEASURE on WMP ($F_{2,28} = 3.90$, $p = 0.03$). Specifically, post-hoc testing revealed a significant caudal difference in the WMP of N15 relative to the WMP of the second iTEP peak ($t = 2.65$, $p = 0.03$) (**Figure S7C**). However, a linear regression model testing the relationship between the WMPs of the N15 and the iTEP peaks revealed an overall weak association ($F = 0.89$, $p = 0.43$), with an R^2 of 0.13 (**Figure S7D**).

Prompted by a reviewer, we explored the relationship between canonical TEP peaks and iTEP peak-to-trough amplitude (**Figure S9**). After stepwise backward model building and Bonferroni correcting for multiple comparisons, we could not demonstrate a linear relation between the iTEPs on the N15 ($F = 0.50$, $p = 1.00$, $R^2 = 0.04$), P30 ($F = 5.91$, $p = 0.15$, $R^2 = 0.33$), and N100 peak ($F = 5.96$, $p = 0.15$, $R^2 = 0.33$). Conversely, there was a main effect of iTEP peak 1 and peak 2 on the N45 ($F = 9.05$, $p = 0.025$, $R^2 = 0.62$) and P60 peak ($F = 13.8$, $p = 0.005$, $R^2 = 0.72$).

Together, these analyses revealed site-specific spatial expression of the early N15 component, mirroring the pericentral crescendo–decrescendo pattern observed in iTEPs, although their magnitudes were unrelated. In contrast, later TEP components showed no site-specificity, but amplitudes of two medium-latency components (i.e., N45 and P60) scaled positively with iTEP peak magnitude.

4. Discussion

This is the first systematic examination of the rostro-caudal iTEP expression evoked with single-pulse TMS of the left pericentral hand region. In agreement with our hypothesis, our linear TMS-EEG mapping approach revealed that iTEPs peaked at the $SM1_{HAND}$ hotspot and diminished rostrally and caudally with increasing distance. While rostro-caudal representation of iTEPs and MEPs were closely correlated across stimulation sites, normalized iTEP amplitudes decayed less rapidly than normalized MEP amplitudes in the caudal direction.

4.1. The iTEP response peaks at pericentral stimulation sites

The iTEPs diminished with increasing distance from the $SM1_{HAND}$ hotspot. This supports the notion that, given the current stimulation intensity and coil orientation, the cortical circuitries capable of generating the characteristic high-frequency iTEP response pattern are located within the pericentral area (Ziemann, 2020). In accordance with our initial report, the temporal iTEP features resemble the rhythmicity of indirect descending corticospinal waves (I-waves) (Beck et al., 2024). Findings in non-human primates suggest that stimulation of both premotor and somatosensory areas can evoke I-waves via afferent input to the primary motor cortex (Shimazu et al., 2004; Patton and Amassian, 1954; Amassian and Stewart, 2003; Baker et al., 2003). Moreover, both electrical stimulation of a peripheral nerve and tactile stimulation of glabrous skin evoke high-frequency activity in S1 in human and non-human primates (Curio et al., 1994; Tomasevic et al., 2022). Accordingly, iTEPs could still be evoked by stimulation over premotor (i.e., rostral) and somatosensory areas (i.e., caudal) in the present study, but this could also be attributed to spatial spread of the electrical field to the primary (sensori)motor hand area.

4.2. Rostro-caudal cortical iTEP and MEP maps are similar but not identical

Our results, showing similar rostro-caudal excitability profiles of iTEPs and MEPs, support the notion that iTEPs reflect a cortical signature of TMS-evoked corticospinal volleys. The inter-individual association between the WMP derived from the iTEP and MEP excitability profiles further suggests neighboring or shared neural generators. We also observed a slight caudal difference in the local iTEP peak maximum relative to the MEP due to a slower postcentral decay of iTEPs relative to MEPs. This finding suggests a postcentral expansion of the cortical representation of iTEPs relative to the corticospinal representation probed with MEP measurements, as normalized iTEP amplitudes decay less rapidly than normalized MEP amplitudes in the caudal direction. This finding extends our recent finding obtained with sulcus-aligned corticomotor mapping of the intrinsic hand muscles, involving MEP measures of SICF (Madsen et al., 2025). Sulcus-aligned corticomotor mapping revealed a caudal shift in the WMP of motor maps when generated with SICF adjusted paired-pulse relative to single-pulse TMS (Madsen et al., 2025). Together, these results suggest that single-pulse MEPs and multi-peak responses, evoked using single-pulse iTEPs and paired-pulse SICF, are generated by overlapping but distinct neural populations.

The exact neural origin of the pericentral multi-peak iTEP remains elusive. The robust signal-to-noise ratio and high amplitude of the pericentral iTEPs indicate a high degree of neuronal synchrony and are compatible with the notion that highly synchronized transsynaptic excitation of large projection neurons, including fast-conducting monosynaptic corticospinal neurons, play a significant, though likely not exclusive, role (Siebner et al., 2022). Of note, peripheral somatosensory stimulation can also evoke high-frequency, multi-peak EEG responses in the pericentral cortex, but this requires a much higher number of peripheral stimuli due to a relative low signal-to-noise ratio (Curio et al., 1994; Tomasevic et al., 2022). The fact that prominent high-frequency iTEPs are only elicited by TMS over pericentral regions should not be taken as evidence that EEG is insensitive to immediate TMS-evoked postsynaptic potentials in more superficial or less geometrically aligned cortical populations. Rather, this underscores the need for future research to determine whether TMS outside the pericentral cortex can evoke more subtle or less synchronized immediate TEPs, potentially resembling the classical components of cortical evoked potentials.

4.3. Studying cortical physiology with subthreshold TMS

As shown in Fig. 4**A**, iTEPs could be elicited in the absence of MEPs in several subjects, particularly at rostral and caudal stimulation sites. This observation may reflect the activation of non-motor cortical regions generating iTEPs, stimulation of neurons projecting to other muscles than the FDI, or the fact that iTEPs can be generated at subthreshold intensities to the resting muscle. Supporting the latter, epidural recordings have consistently shown that I-waves can be elicited below the rMT (Di Lazzaro et al., 1998). Keeping with this line of reasoning, our previous work testing the input-output relationship of iTEPs demonstrated their emergence at stimulation intensities between the active and resting motor thresholds (Beck et al., 2024).

Overall, these results highlight that the presence of iTEPs are a direct marker of the immediate pericentral response to TMS even in the absence of an overt muscle response (i.e., MEPs). This opens new possibilities to study pericentral cortical excitability in patient groups with corticomotor pathology, in whom MEPs cannot be obtained.

4.4. The relationship between immediate and standard TEP components at later latencies

Single-pulse stimulation over the six frontoparietal cortical sites evoked the well-known cascade of TEPs, including the N15, P30, N45, P60, and N100 (Fig. 2**F** and **Figure S6**) (Beck et al., 2024; Ilmoniemi and Kičić, 2010; Farzan et al., 2016; Hill et al., 2016). While the highly site-specific iTEPs are a direct pericentral response to the TMS pulse, reflecting local cortical excitability, the later TEP components can be attributed to transsynaptic spread, causing recurrent activation in both local and remote brain regions, alongside non-transcranial

co-activations via multisensory peripheral inputs (Bortoletto et al., 2015; Conde et al., 2019).

The iTEPs and the early N15 peak showed a rostro-caudal crescendo-decrescendo pattern with a clear pericentral peak expression. This close spatial alignment was not paralleled by a covariation in amplitude, as we found no relationship between the iTEP peak-to-through and N15 magnitude. Although this cannot be taken as definitive proof that the N15 and iTEPs reflect distinct neural processes, additional lines of evidence support such interpretation. Intracortical recordings in rodents showed that single-pulse TMS with a posterior to anterior (PA) current induced high-frequency spiking consistent with iTEPs, as well as later activity from 15 to 35 ms (Li et al., 2017). In contrast, a medial to lateral current orientation only evoked later activity 15 ms (Li et al., 2017), suggesting that the neural activity around 15 ms can be evoked without evoking immediate spiking in cortical pyramidal cells. In humans, a biphasic anterior-to-posterior (AP) current orientation evoked MEPs with longer onset latencies but N15 components with shorter peak latencies compared to biphasic posterior-to-anterior (PA) current orientation (Lucarelli et al., 2025). Together, the existing data supports the notion that the early N15 component is not a 'downstream' effect triggered by the highly synchronized pericentral activity constituting the high frequency iTEP response.

The statistical absence of a site-specific effect on later TEP components (> 15 ms) suggests that the synchronized evoked activity operating at these intervals may have a wider spatial representation involving not only the pericentral region (Bortoletto et al., 2015; Conde et al., 2019). While some degree of site specificity in the latency, polarity, and magnitude of later TEP peaks is expected (Rosanova et al., 2009; Fecchio et al., 2025; Passera et al., 2022), it has been demonstrated that TMS-evoked EEG features can be shared between stimulation sites separated by several centimeters (Passera et al., 2022). Hence, our linear mapping approach may have been too rigid to detect such distinctive features.

Exploratory analyses prompted by a reviewer revealed significant associations between iTEP peak-to-trough amplitudes and two medium-latency TEP components (i.e., N45 and P60). While this may indicate a causal relationship, the complexity of later TEPs precludes a definitive interpretation. Potential contributing factors include intra-individual noise, interindividual variability in signal-to-noise ratio, and non-transcranial co-activation via multisensory peripheral inputs, such as feedback activation from TMS-evoked muscle twitches (Bortoletto et al., 2015; Conde et al., 2019). Since the experimental design was not optimized for exploratory analyses of later TEP components, future research is needed to disentangle the complex relationship between immediate (iTEPs), early (N15), and later (>15 ms) TEP responses.

4.5. *Methodological considerations and recommendations for future work*

Our experimental design only allows a rough localization of the maximal iTEP expression across stimulation sites, because we did not systematically optimize TMS parameters such as coil orientation and stimulus intensity, across all stimulus locations. Future studies may benefit from a more fine-grained systematic examination of how specific TMS parameters impact the regional iTEP expression at specific stimulus locations (Casarotto et al., 2022). For instance, we cannot rule out that the absence of MEPs or iTEPs over more rostral and caudal stimulus locations resulted from an insufficient stimulus intensity, a suboptimal pulse configuration or current direction. It would also be worthwhile in future studies to calculate the spatial distributions of the TMS-induced electrical fields and relate them with the iTEP magnitudes (Weise et al., 2023). Keeping with this line of reasoning, stimulation of premotor areas is known to contribute to I-wave generation via afferent input to M1 (Shimazu et al., 2004; Schmidlin et al., 2008). Hence, it would be worthwhile for future studies to explore the cortico-cortical contribution to iTEPs through a multi-coil setup (Nieminen et al., 2022).

Future studies need to explore strategies to minimize decay artifacts, particularly when studying responses at early latencies. The current study showed that these artifacts significantly impact the window to detecting results. Hence, considering hardware specifications, maintaining low impedances, and aligning the electrode lead orientation relative to the TMS coil may be important to mitigate their impact in future research (Hernandez-Pavon et al., 2023).

We used a 2-second ITI with ± 10 % jitter to ensure a sufficient number of trials for reliable (i)TEP quantification, in line with current TMS-EEG guidelines (Hernandez-Pavon et al., 2023) and common practice in the broader TMS-EEG literature (Beck et al., 2024). A 2-second intertrial interval also minimized participant burden but may not have been sufficiently long to prevent potential carry-over effects on MEPs from preceding TMS pulses (Pellicciari et al., 2016; Bonnesen et al., 2022). In accordance with this, the use of a sequential stimulation order across rostro-caudal stimulation sites may have introduced order-related effects potentially influencing measures of cortical and/or corticospinal excitability.

5. Conclusion

Linear rostro-caudal mapping revealed that the characteristic iTEPs peak at the $SM1_{HAND}$ hotspot and decrease rostrally and caudally with increasing distance. The MEPs of contralateral hand muscles exhibit a similar crescendo-decrescendo pattern. Together, these results support the hypothesis that iTEPs reflect a direct response signature of the pericentral cortex, possibly involving a synchronized excitation of pyramidal tract neurons. The rostro-caudal iTEP and MEP maps were very similar but not identical. At the first postcentral site, normalized iTEPs showed a stronger magnitude relative to the normalized MEPs, suggesting that pericentral iTEPs and MEPs may be generated by overlapping but distinct neuron populations.

CRediT authorship contribution statement

Marten Nuyts: Writing – review & editing, Writing – original draft, Visualization, Validation, Software, Project administration, Methodology, Investigation, Funding acquisition, Formal analysis, Data curation, Conceptualization. **Mikkel Malling Beck:** Visualization, Validation, Software, Resources, Project administration, Methodology, Investigation, Formal analysis, Conceptualization. **Agata Banach:** Investigation. **Axel Thielscher:** Writing – review & editing. **Raf Meesen:** Writing – review & editing, Supervision, Resources, Funding acquisition. **Leo Tomasevic:** Writing – review & editing, Visualization, Validation, Software, Formal analysis. **Hartwig Roman Siebner:** Writing – review & editing, Visualization, Validation, Supervision, Resources, Project administration, Methodology, Funding acquisition, Conceptualization. **Lasse Christiansen:** Writing – review & editing, Visualization, Validation, Supervision, Software, Resources, Project administration, Methodology, Investigation, Funding acquisition, Conceptualization.

Declaration of competing interest

Hartwig Roman Siebner received honoraria as speaker and consultant from Lundbeck AS, Denmark, and as editor (Neuroimage Clinical) from Elsevier Publishers, Amsterdam, The Netherlands. He has received royalties as book editor from Springer Publishers, Stuttgart, Germany, Oxford University Press, Oxford, UK, and from Gyldendal Publishers, Copenhagen, Denmark. All other authors declare to have no known conflicts of interest or competing interests.

Funding statement

Marten Nuyts holds a Fundamental Research Grant (grant no. 11PBG24N) and Travel Grant: Long-Stay Abroad (grant no. V416924N) by Research Foundation Flanders. Mikkel M. Beck is funded by a postdoc grant from the Capital Region Denmark (Region H) and holds a postdoc

grant from The Lundbeck Foundation (grant no. R449-2023-1487). Axel Thielscher was supported by the Lundbeck Foundation (grants R313-2019-622 and R244-2017-196). Leo Tomasevic holds an 'Experiment grant' from The Lundbeck Foundation (grant no. R346-2020-1822) and was partially funded by the dtec.bw – Digitalization and Technology Research Center of the Bundeswehr [MEXT project]. Hartwig Roman Siebner and Axel Thielscher have received funding for the project "Precision Brain-Circuit Therapy - Precision-BCT" from Innovation Funds Denmark (grant nr. 9068-00025B). Hartwig Roman Siebner has received funding the project "ADAptive and Precise Targeting of cortex-basal ganglia circuits in Parkinsonś Disease - ADAPT-PD" from Lundbeckfonden (collaborative project grant, grant nr. R336-2020-1035).

Acknowledgments

We would like to thank Sybren Van Hoornweder for the insightful discussions and acknowledge Ditte Haagerup and Kora Montemagno for their support in setting up the experiment. We also thank the reviewers for their constructive feedback, particularly the suggestions to include the conventional later TEP components in our analysis and explore their relationship with the iTEPs.

Data and code availability statement

The data that support the findings of this study are available from the corresponding authors, Marten Nuyts and Lasse Christiansen, upon reasonable request.

Supplementary materials

Supplementary material associated with this article can be found, in the online version, at doi:10.1016/j.neuroimage.2025.121446.

Data availability

Data will be made available on request.

References

Amassian, V.E., Stewart, M., 2003. Motor cortical and other cortical interneuronal networks that generate very high frequency waves. Suppl. Clin. Neurophysiol. 56, 119–142.
Baker, S.N., Gabriel, C., Lemon, R.N., 2003. EEG oscillations at 600 hz are macroscopic markers for cortical spike bursts. J. Physiol. 550 (2), 529–534.
Bates, D., et al., 2015. Fitting linear mixed-effects models using lme4. J. Stat. Softw. 67 (1), 1–48.
Beck, M.M., et al., 2023. Gain function and state dependency of transcranial evoked potentials elicited by single-pulse TMS of the primary motor cortex. Brain Stimul. 16 (1), 293.
Beck, Mikkel M., et al., 2024a. Methodological choices matter: a systematic comparison of TMS-EEG studies targeting the primary motor cortex. Hum. Brain Mapp. 45 (15), e70048.
Beck, M.M., et al., 2024b. Transcranial magnetic stimulation of primary motor cortex elicits an immediate transcranial evoked potential. Brain Stimul. 17 (4), 802–812.
Beck, M., et al., Methodological choices matter: a systematic comparison of TMS-EEG studies targeting the primary motor cortex. 2024c.
Bonnesen, M.T., et al., 2022. The recent history of afferent stimulation modulates corticospinal excitability. Neuroimage 258, 119365.
Bortoletto, M., et al., 2015. The contribution of TMS-EEG coregistration in the exploration of the human cortical connectome. Neurosci. Biobehav. Rev. 49, 114–124.
Casarotto, S., et al., 2022. The rt-TEP tool: real-time visualization of TMS-evoked potentials to maximize cortical activation and minimize artifacts. J. Neurosci. Methods 370, 109486.
Conde, V., et al., 2019. The non-transcranial TMS-evoked potential is an inherent source of ambiguity in TMS-EEG studies. Neuroimage 185, 300–312.
Curio, G., et al., 1994. Localization of evoked neuromagnetic 600 hz activity in the cerebral somatosensory system. Electroencephalogr. Clin. Neurophysiol. 91 (6), 483–487.
Delorme, A., Makeig, S., 2004. EEGLAB: an open source toolbox for analysis of single-trial EEG dynamics including independent component analysis. J. Neurosci. Methods 134 (1), 9–21.
Di Lazzaro, V., Rothwell, J.C., 2014. Corticospinal activity evoked and modulated by non-invasive stimulation of the intact human motor cortex. J. Physiol. 592 (19), 4115–4128.
Di Lazzaro, V., et al., 1998. Comparison of descending volleys evoked by transcranial magnetic and electric stimulation in conscious humans. Electroencephalogr. Clin. Neurophysiol. 109 (5), 397–401.
Farzan, F., Bortoletto, M., 2022. Identification and verification of a 'true' TMS evoked potential in TMS-EEG. J. Neurosci. Methods 378, 109651.
Farzan, F., et al., 2016. Characterizing and modulating brain circuitry through transcranial magnetic stimulation combined with electroencephalography. Front. Neural Circuits 10, 73.
Fecchio, M., et al., The spatiotemporal evolution of TMS-evoked potentials reflects direct cortical activation. bioRxiv, 2025: p. 2025.06.25.661535.
Hernandez-Pavon, J.C., et al., 2023. TMS combined with EEG: recommendations and open issues for data collection and analysis. Brain Stimul. 16 (2), 567–593.
Hill, A.T., et al., 2016. TMS-EEG: a window into the neurophysiological effects of transcranial electrical stimulation in non-motor brain regions. Neurosci. Biobehav. Rev. 64, 175–184.
Ilmoniemi, R.J., Kičić, D., 2010. Methodology for combined TMS and EEG. Brain Topogr. 22 (4), 233–248.
Ilmoniemi, R.J., et al., 1997. Neuronal responses to magnetic stimulation reveal cortical reactivity and connectivity. NeuroReport 8 (16).
Kähkönen, S., et al., 2005. Prefrontal transcranial magnetic stimulation produces intensity-dependent EEG responses in humans. Neuroimage 24 (4), 955–960.
Kammer, T., et al., 2001. Motor thresholds in humans: a transcranial magnetic stimulation study comparing different pulse waveforms, current directions and stimulator types. Clin. Neurophysiol. 112 (2), 250–258.
Lehmann, D., Skrandies, W., 1980. Reference-free identification of components of checkerboard-evoked multichannel potential fields. Electroencephalogr. Clin. Neurophysiol. 48 (6), 609–621.
Li, B., et al., 2017. Lifting the veil on the dynamics of neuronal activities evoked by transcranial magnetic stimulation. Elife 6.
Lucarelli, D., et al., 2025. Stimulation parameters recruit distinct cortico-cortical pathways: insights from microstate analysis on TMS-evoked potentials. Brain Topogr. 38 (3), 39.
Madsen, M.A.J., et al., 2025. Single and paired TMS pulses engage spatially distinct corticomotor representations in human pericentral cortex. J. Neurophysiol. 133 (5), 1423–1434.
Mueller, J.K., et al., 2014. Simultaneous transcranial magnetic stimulation and single-neuron recording in alert non-human primates. Nat. Neurosci. 17 (8), 1130–1136.
Mutanen, T., Mäki, H., Ilmoniemi, R.J., 2013. The effect of stimulus parameters on TMS-EEG muscle artifacts. Brain Stimul. 6 (3), 371–376.
Nieminen, J.O., et al., 2022. Multi-locus transcranial magnetic stimulation system for electronically targeted brain stimulation. Brain Stimul. 15 (1), 116–124.
Oostenveld, R., et al., 2011. FieldTrip: open source software for advanced analysis of MEG, EEG, and invasive electrophysiological data. Comput. Intell. Neurosci. 2011, 156869.
Passera, B., et al., 2022. Exploring the spatial resolution of TMS-EEG coupling on the sensorimotor region. Neuroimage 259, 119419.
Patil, I., 2021. Visualizations with statistical details: the 'ggstatsplot' approach. J. Open Source Softw. 6, 3167.
Patton, H.D., Amassian, V.E., 1954. Single and multiple-unit analysis of cortical stage of pyramidal tract activation. J. Neurophysiol. 17 (4), 345–363.
Pellicciari, M.C., et al., 2016. Ongoing cumulative effects of single TMS pulses on corticospinal excitability: an intra- and inter-block investigation. Clin. Neurophysiol. 127 (1), 621–628.
Raffin, E., et al., 2015. Bringing transcranial mapping into shape: sulcus-aligned mapping captures motor somatotopy in human primary motor hand area. Neuroimage 120, 164–175.
Rosanova, M., et al., 2009. Natural frequencies of human corticothalamic circuits. J. Neurosci. 29 (24), 7679–7685.
RStudio, P., RStudio: integrated development environment for R. 2020.
RStudio, P., R: a language and environment for statistical computing. 2021.
Russo, S., et al., 2022. TAAC - TMS adaptable auditory control: a universal tool to mask TMS clicks. J. Neurosci. Methods 370, 109491.
Schmidlin, E., et al., 2008. Pronounced reduction of digit motor responses evoked from macaque ventral premotor cortex after reversible inactivation of the primary motor cortex hand area. J. Neurosci. 28 (22), 5772–5783.
Shimazu, H., et al., 2004. Macaque ventral premotor cortex exerts powerful facilitation of motor cortex outputs to upper limb motoneurons. J. Neurosci. 24 (5), 1200–1211.
Siebner, H.R., et al., 2022. Transcranial magnetic stimulation of the brain: what is stimulated? - a consensus and critical position paper. Clin. Neurophysiol. 140, 59–97.
Smith, S.M., Nichols, T.E., 2009. Threshold-free cluster enhancement: addressing problems of smoothing, threshold dependence and localisation in cluster inference. Neuroimage 44 (1), 83–98.
Sommer, M., et al., 2006. Half sine, monophasic and biphasic transcranial magnetic stimulation of the human motor cortex. Clin. Neurophysiol. 117 (4), 838–844.

Stango, A., et al., Immediate TMS-EEG responses reveal motor cortex excitability. bioRxiv, 2024: p. 2024.08.20.608770.
Tomasevic, L., Takemi, M., Siebner, H.R., 2017. Synchronizing the transcranial magnetic pulse with electroencephalographic recordings effectively reduces inter-trial variability of the pulse artefact. PLoS One 12 (9), e0185154.
Tomasevic, L., et al., 2022. Relationship between high-frequency activity in the cortical sensory and the motor hand areas, and their myelin content. Brain Stimul. 15 (3), 717–726.
Van Hoornweder, S., et al., 2025. The causal role of beta band desynchronization: Individualized high-definition transcranial alternating current stimulation improves bimanual motor control. Neuroimage 312, 121222.
Veniero, D., Bortoletto, M., Miniussi, C., 2009. TMS-EEG co-registration: on TMS-induced artifact. Clin. Neurophysiol. 120 (7), 1392–1399.
Weise, K., et al., 2023. Precise motor mapping with transcranial magnetic stimulation. Nat. Protoc. 18 (2), 293–318.
Yousry, T.A., et al., 1997. Localization of the motor hand area to a knob on the precentral gyrus. A new landmark. Brain 120 (Pt 1), 141–157.
Ziemann, U., et al., 1998. Demonstration of facilitatory I wave interaction in the human motor cortex by paired transcranial magnetic stimulation. J. Physiol. 511 (Pt 1), 181–190 (Pt 1).
Ziemann, U., 2020. I-waves in motor cortex revisited. Exp. Brain Res. 238 (7–8), 1601–1610.